Improving the Efficiency of Multilayer Organic Light-Emitting Transistors by Exploring the Hole Blocking Effect

Yongsheng Hu, Li Song,* ShiTong Zhang, Ying Lv, Jie Lin, Xiaoyang Guo, and Xingyuan Liu*

Organic light-emitting transistors (OLETs) are emerging as a type of multi-functional devices that integrate the electrical switching and the light-emitting function. Among the various device structures, multilayer OLETs have shown superior performance due to their flexibility in structure design and material choice. However, multilayer OLETs usually work in the unipolar mode, resulting in extreme unbalance between the holes and electrons, restricting the further improvement of their performance. Here, an investigation of the hole blocking layer (HBL) is presented. The results show that a high electron mobility is not necessarily in a first place when choosing the HBL, while a deeper highest occupied molecular orbital level of the HBL can better facilitate the exciton recombination efficiency. By using bis[(4-tert-butylphenyl)-1,3,4-oxadiazolyl]phenylene instead of commonly used bathophenanthroline (Bphen) as the HBL, the external quantum efficiency (EQE) is more than doubled for a blue fluorescent OLET, and an EQE as high as 10.3% is achieved in a green phosphorescent OLET with a maximum brightness of ≈8000 cd m^{-2}. The findings in this work highlight the importance of carrier blocking in building high efficiency OLETs and might provide some guidance for their structure design and material choice.

1. Introduction

Organic light-emitting transistors (OLETs) have gained wide attention due to their integrated switching function of field-effect transistors and luminescence function of organic light-emitting devices (OLEDs), which enable them fascinating applications in the fields of flat panel displays, optical communication, sensors, and potentially, electrically driven organic lasers.[1,2] During the past decade, great efforts have been made to improve the performance of the OLETs. For instance, various organic materials with high carrier mobilities,[3–6] high photoluminescence quantum yield (PLQY),[7–9] and exciton utility efficiency[10–13] have been adopted or developed; different device structures[14,15] and interfacial/surface modification strategies[16,17] facilitating the injection/transport of carriers have also been investigated. Despite the great progress in both optical and electrical performance for the OLETs, due to the lack of organic materials with both high PLQY and high mobilities, and the inefficient injection/transport of carriers, there is still a large gap from practical applications.

Among the various device structures, multilayer OLETs consisting of an emissive layer and a p-type and/or an n-type carrier transport layer rather than a single active layer show high flexibility in structure design and material choice.[16,18] By employing materials with high mobility as the carrier transport layer and with high PLQY as the emissive layer, respectively, multilayer OLETs can well balance the carrier transport and the radiation recombination, thus enable a relatively high external quantum efficiency (EQE). However, due to the lack of organic carrier transport materials with high mobility, the EQE of multilayer OLETs is still restricted by the minority carriers (electrons), which causes inefficient exciton recombination in the emissive layer, as evidenced by localized charge carrier recombination near the drain electrode region where the minority carriers are injected in most cases.[14,16] Therefore, further promoting the exciton recombination in the emission layer is desired for achieving efficient multilayer OLETs.

One common route to promoting the exciton recombination is to improve the injection of the minority carriers by adopting low work function electrodes or electrode modifications.[17,19,20]

Dr. Y. Hu, Dr. Y. Lv, Dr. J. Lin, Dr. X. Guo, Prof. X. Liu
State Key Laboratory of Luminescence and Applications
Changchun Institute of Optics
Fine Mechanics and Physics
Chinese Academy of Sciences
Changchun 130033, China
E-mail: liuxy@ciomp.ac.cn

Dr. L. Song
Tianjin Key Laboratory of Electronic Materials and Devices
School of Electronics and Information Engineering
Hebei University of Technology
Tianjin 300401, China
E-mail: songli@hebut.edu.cn

Dr. S. Zhang
State Key Laboratory of Supramolecular Structure and Materials
Jilin University
Changchun 130012, China

Prof. X. Liu
Center of Materials Science and Optoelectronics Engineering
University of Chinese Academy of Sciences
Beijing 100049, China

The ORCID identification number(s) for the author(s) of this article can be found under https://doi.org/10.1002/admi.202000657.
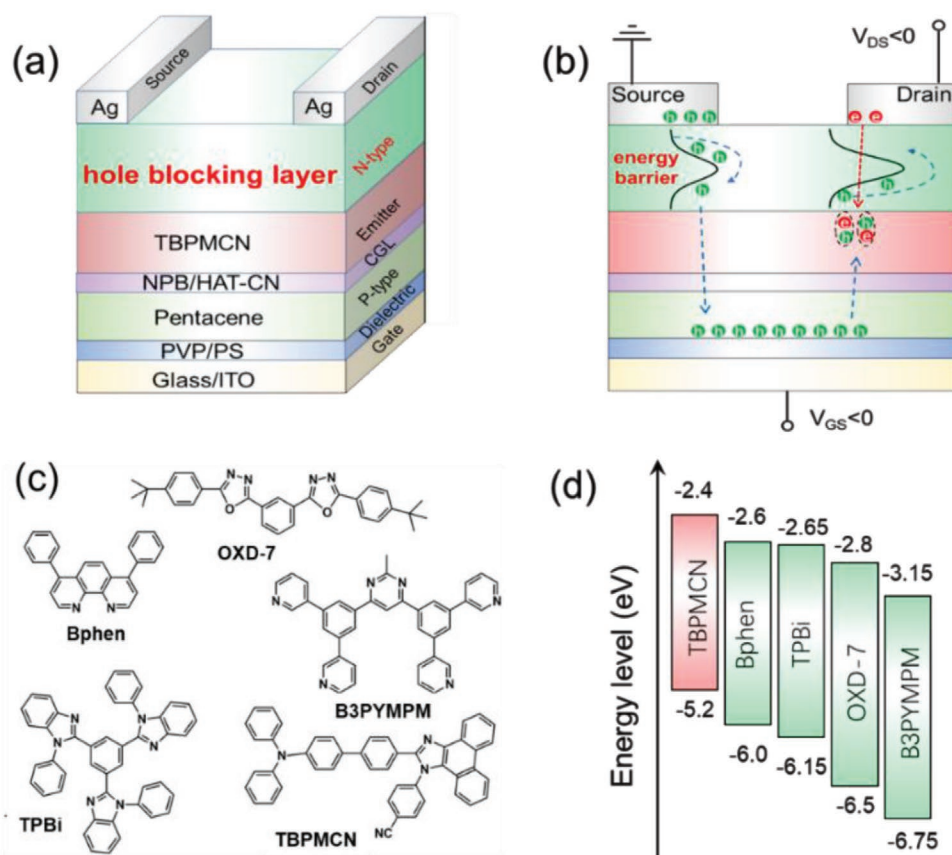
Figure 1. a) Schematic structure of the device. b) Schematic diagram of the injection and transport of the carriers. c) Molecular structures and d) electronic energy levels of the four HBL materials and TBPMCN.

Another feasible route is to suppress the transport of majority carriers so that the excitons can be better restricted in the emission layer. In principle, holes can be well blocked by using electron transport materials which have a deep highest occupied molecular orbital (HOMO) level, as has been widely studied in OLEDs,[21,22] whereas in the horizontally configured OLETs, this is not easy because when the holes that escape from the emission layer beneath the drain electrode are blocked, those injected from the source electrode will also suffer an energy barrier and be blocked (**Figure 1**b), possibly leading to a deterioration of hole transport and device performance. Consequently, few studies have concentrated on the hole blocking layer (HBL) so far[12,23] and the hole blocking effect has not been fully explored and utilized for the multilayer OLETs.

In previous studies, we have demonstrated that the hole transport ability of multilayer OLETs can be significantly enhanced by adopting a charge generation layer (CGL),[11,16] thus be less affected by the hole injection process beneath the source electrode. Unfortunately, the increased hole mobility also brought an overbalance between the holes and electrons in the channel, leading to a limited emission efficiency. We anticipated to further improve the optical performance of multilayer OLETs by restricting the hole transport beneath the drain electrode. Hence, here we focused on the HBL and investigated the influence of HBL properties, including energy levels, mobility, and thickness. The results show that a high electron mobility is

not necessarily in a first place when choosing the HBL, while a deeper HOMO level can better facilitate the hole blocking effect of the HBL and promote the exciton recombination efficiency. Besides, the thickness and lowest unoccupied molecular orbital (LUMO) level of the HBL also play essential roles. By using bis[(4-tert-butylphenyl)-1,3,4-oxadiazolyl]phenylene (OXD-7) instead of commonly used bathophenanthroline (Bphen) as the HBL, the EQE is more than doubled for a blue fluorescent OLET and an EQE exceeding 10% has been achieved for the first time in a phosphorescent OLET. The findings in this work might provide some guidance for the structure design and material choice in building high efficiency OLETs and pave a way for their practical use in the future.

2. Results and Discussion

Figure 1a presents the schematic structure of the device, which was fabricated by using poly-4-vinylphenol (PVP)/polystyrene (PS) as the dielectric on indium tin oxide (ITO) substrate. Pentacene was used as the hole transport layer due to its high mobility. *N*,*N*′-di(naphthalene-1-yl)-*N*,*N*′-diphenyl-benzidine (NPB)/1,4,5,8,9,11-hexaazatriphenylene hexacarbonitrile (HAT-CN) acted as the CGL. The molecular structure and electronic energy levels of the materials are shown in Figure S1 in the Supporting Information. A deep blue fluorescent material

**ADVANCED
SCIENCE NEWS**

www.advancedsciencenews.com

**ADVANCED
MATERIALS
INTERFACES**

www.advmatinterfaces.de

Table 1. HOMO/LUMO levels and electron mobilities for the four HBL materials and TBPMCN.

HBLs	TBPMCN	Bphen	TPBi	OXD-7	B3PYMPM
HOMO [eV]	−5.2[24]	−6.0[25]	−6.15[25]	−6.5[22]	−6.75[25]
LUMO [eV]	−2.4[24]	−2.6[25]	−2.65[25]	−2.8[22]	−3.15[25]
Mobility [cm^2 V^{-1} s^{-1}]	NA	$(2.4–5.2) \times 10^{-4[26,27]}$	$(3.3–8) \times 10^{-5[28]}$	$2.1 \times 10^{-5[26]}$	$1.5 \times 10^{-5[29]}$

4-[2-(4′-diphenylamino-biphenyl-4-yl)-phenanthro[9,10-d]imi-dazol-1-yl]-benzonitrile (TBPMCN) was chosen as the emitter due to its high exciton utility efficiency as a result of the harvest of triplet excitons through hybridized local and charge-transfer excited state.[24] The absorption and photoluminescence spectra of TBPMCN film are shown in Figure S2 in the Supporting Information. Cs_2CO_3 (1 nm)/Al (1 nm) modified[11] Ag (50 nm) was used as the source and drain electrodes.

As for the HBL, a commonly used electron transport material Bphen was in a first place considered due to its relatively high electron mobility (**Table 1**) and much deeper HOMO level (−6.0 eV) than that of TBPMCN (−5.2 eV). However, the device did not show a high emission efficiency with an EQE of only ≈0.5% (**Table 2**). We speculated that the excitons might not be well formed in the emission layer for the device. To verify this, a thin layer (5 nm) of 4,4′-bis(carbazol-9-yl) biphenyl (CBP) was inserted either prior to or after the emission layer as an indicator. As shown in Figure S3 in the Supporting Information, when CBP was inserted between the emitter and the CGL, the electroluminescence (EL) spectrum kept the same as that without CBP, showing an emission peak at 442 nm which was originated from TBPMCN. However, when CBP was inserted between the emitter and the HBL, a new emission peak originated from CBP appeared. Such a result indicates that the excitons were mainly formed at the interface of Bphen/TBPMCN, suggesting that the holes

were not well restricted in the emission layer. Therefore, we further considered another three commercial electron transport materials with deeper HOMO levels as new HBLs, which are 1,3,5-tris(2-N-phenylbenzimidazolyl) benzene (TPBi), OXD-7, and bis-4,6-(3,5-di-3-pyridylphenyl)-2-methylpyrimi-dine (B3PYMPM). The molecular structures, electronic energy levels, and electron mobilities of the four HBL materials and TBPMCN are listed in Figure 1c,d and Table 1.

We first analyze the hole blocking effect on the electrical performance of the devices. **Figure 2**a–d shows the transfer characteristics at the drain to source voltage $V_{DS} = −100$ V for devices with the 4 different HBLs. All the devices exhibit a typical p-type characteristic with a high on/off ratio >10^5. The p-type characteristic can be also found from the output curves (Figure S4, Supporting Information). The p-type characteristic indicate that all the devices are working under the hole-dominating mode, which is expectable since the electron mobilities of the four HBL materials are much lower compared to the hole mobility of pentacene.[30] The strong hole-dominating property leads to a localized emission area at the vicinity of the drain electrode for all the devices (Figure S5, Supporting Information). A schematic diagram of the injection and transport of the carriers for the hole-dominating mode is shown in Figure 1b (and Figure S6, Supporting Information). Holes are injected from the source electrode, and then transport across the channel and finally recombine with electrons injected from the

Table 2. Summary of the electrical and optical characteristics for TBPMCN based OLETs with different HBLs.

HBLs	Thickness [nm]	hole mobility [cm^2 V^{-1} s^{-1}]	V_{th} [V]	EQE$_{max}$ [%]	L_{max} [cd m^{-2}]	Recombination efficiency$^{a)}$ [%]
Bphen	10	0.73	−23	0.36	913	4.5
	20	0.64	−24.4	0.48	973	6.0
	30	0.61	−28	0.54	955	6.6
	40	0.61	−33.9	0.58	939	7.1
TPBi	10	0.46	−26.7	0.11	166	1.3$^{b)}$
	20	0.41	−29.5	0.39	347	3.4
	30	0.31	−33.6	0.58	383	5.6
	40	0.23	−34.8	0.56	320	6.3
OXD-7	10	0.70	−33.9	0.15	298	1.9
	20	0.62	−36.8	0.47	736	5.8
	30	0.29	−38.9	1.39	855	16.3
	40	0.17	−44.3	1.52	509	16.9
B3PYMPM	10	0.80	−40.9	0.64	746	7.1
	20	0.50	−44.4	0.77	810	9.1
	30	0.45	−47.4	1.28	906	15.3
	40	0.38	−48	1.02	603	11.3

$^{a)}$At 300 cd m^{-2}; $^{b)}$At maximum brightness.

**ADVANCED
SCIENCE NEWS**
www.advancedsciencenews.com

**ADVANCED
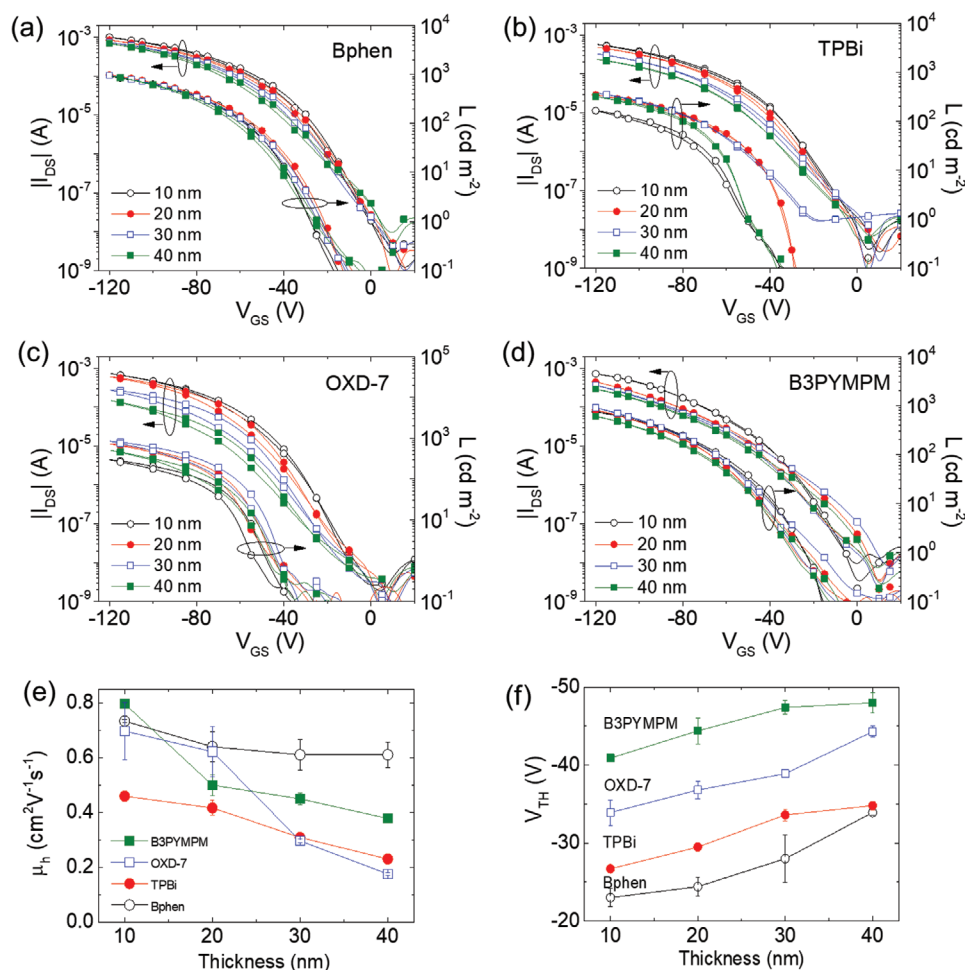MATERIALS
INTERFACES**
www.advmatinterfaces.de

Figure 2. Electrical and optical transfer characteristics for devices with the HBL of a) Bphen, b) TPBi, c) OXD-7, and d) B3PYMPM under different thicknesses from 10 to 40 nm at $V_{DS} = -100$ V . e) Relationship between the hole mobility and the thickness of HBL for different devices. f) Relationship between the threshold voltage and the thickness of HBL for different devices.

drain electrode in the emission layer. The transport route of the carriers suggests there are two distinct energy barriers induced by the HBL. One is at the interface of source electrode/HBL and the other is at the interface of emission layer/HBL beneath the drain electrode. Since both energy barriers can block either the injection or the transport of holes, the channel current is expected to be deteriorated to some degree. However, since the device shows strong hole-dominating property, the above blocks of holes, especially the one at the interface of emission layer/HBL will in turn favor the improvement of the exciton recombination efficiency as an increased charge balance.

The hole transport ability of an OLET can be characterized by the carrier mobility and the threshold voltage (V_{TH}). The hole mobility is derived from the transfer curves in the saturation region by the following equation[31]

$$\mu_{sat} = \frac{2L}{wc_i}\left(\frac{\partial \sqrt{I_{DS}}}{\partial V_{GS}}\right)^2 \tag{1}$$

where W and L represent the channel width and length, respectively, and C_i is the capacitance per unit area of the dielectric

($\approx$4.5 nF cm^{-2}). The threshold voltage can be determined from the relationship between $\sqrt{I_{DS}}$ and V_{GS} as shown in Figure S7 in the Supporting Information. Figure 2e,f presents the hole mobilities and threshold voltages for all the devices. The mobilities for all the devices decrease as the thickness of the HBL increases from 10 to 40 nm. The mobilities change from 0.73 to 0.61 cm^2 V^{-1} s^{-1}, from 0.46 to 0.23 cm^2 V^{-1} s^{-1}, from 0.70 to 0.17 cm^2 V^{-1} s^{-1}, and from 0.80 to 0.38 cm^2 V^{-1} s^{-1} for Bphen, TPBi, OXD-7, and B3PYMPM, respectively (Figure 2e and Table 2). Bphen based devices show the minimal decrease of mobility, which agrees well with its shallow HOMO level. TPBi and OXD-7 based devices show more decrease than that of Bphen based devices, which also coincide well with the change of their HOMO levels. However, B3PYMPM based devices exhibit higher hole mobility and slighter decrease than that of OXD-7 based devices despite its deeper HOMO level than that of OXD-7. We speculate that it may be influenced by the morphology of the films. Figure S8 in the Supporting Information shows the atomic force microscope images for different HBLs deposited on ITO/PVP/PS/pentacene/NPB/HAT-CN/TBPMCN. The root mean square roughness of B3PYMPM (4.19 nm) is

much larger than that of OXD-7 (2.27 nm), which is believed to facilitate the carriers injection and transport.[32]

As the thickness of the HBLs increases, the threshold voltages also exhibit an increment from −23 to −33.9 V, from −26.7 to −34.8 V, from −33.9 to −44.3 V, and from −40.9 to −48 V for Bphen, TPBi, OXD-7, and B3PYMPM based devices, respectively (Figure 2f and Table 2). It is worth noting that the threshold voltages (absolute value) at a certain thickness follow the order: Bphen < TPBi < OXD-7 < B3PYMPM, which agrees well with the change of their HOMO levels. This can be attributed to the increased energy barriers induced by the HBLs beneath both the source and the drain electrodes. These results indicate that the hole transport ability of the multilayer OLETs in this work is closely related to the HOMO level of the HBL as well as its thickness.

Next, we investigate the influence of the hole blocking effect on the emission performance of the devices. Figure 2a–d and **Figure 3** present the brightness and the EQE of the devices,

respectively. Bphen based devices show the highest brightness (≈970 cd m^{-2}) and the brightness is more stable than that of the others as the thickness of HBL increases from 10 to 40 nm. Since the brightness is proportional to EQE and current density ($L \propto$ EQE $\times J$), the high brightness for Bphen based devices can be attributed to their high drain current benefited from the weak hole blocking effect. As the thickness of Bphen increases, the EQE increases gradually from 0.36% to 0.58%, suggesting that the holes and electrons are becoming more balanced as the hole blocking effect beneath both the source and the drain electrodes strengthened. This can be better interpreted by the exciton recombination efficiency of the devices, which can be estimated by the following equation[19]

$$\text{EQE} = \gamma \, \Phi_{\text{spin}} \Phi_{\text{PL}} \Phi_{\text{out}} \tag{2}$$

where γ, Φ_{spin}, Φ_{PL}, and Φ_{out} denote the exciton recombination efficiency, the exciton utilization efficiency, the PLQY of
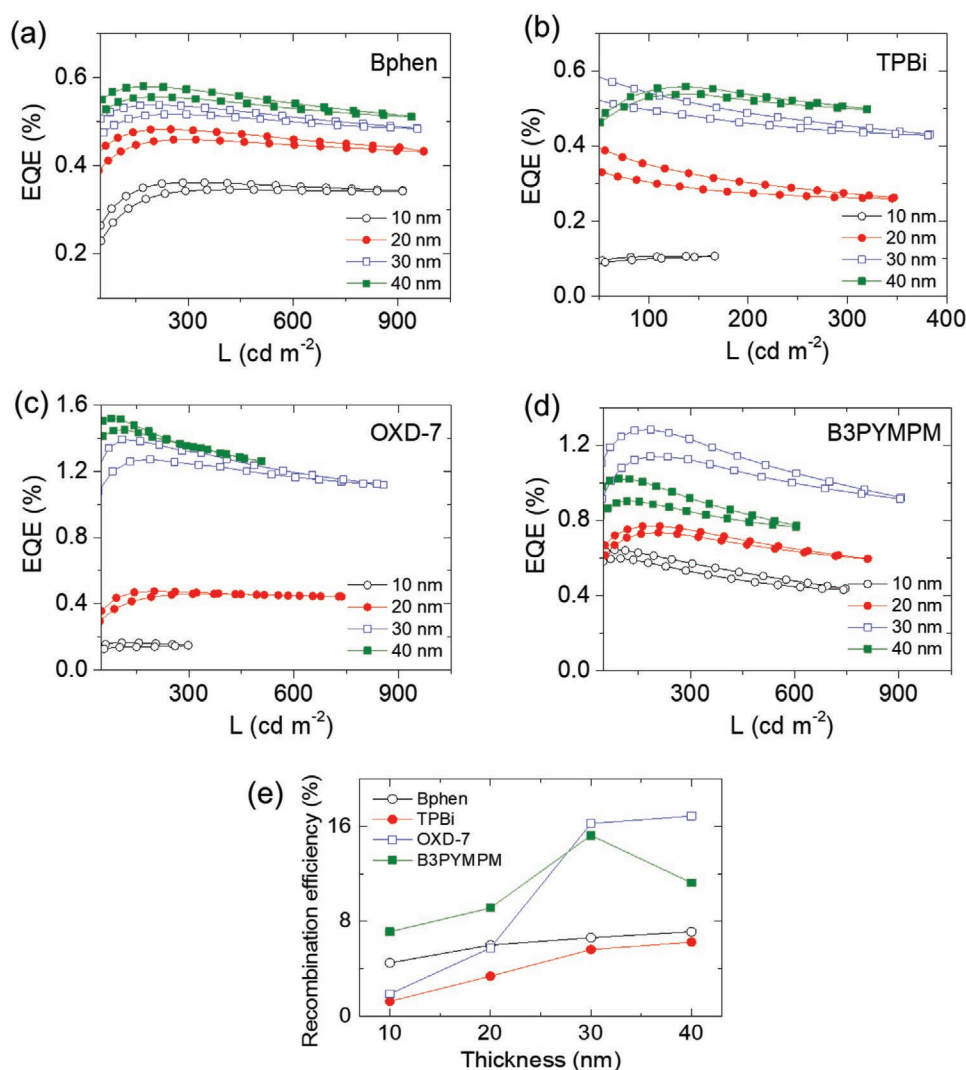

Figure 3. Characteristics of the EQE and brightness for devices with the HBL of a) Bphen, b) TPBi, c) OXD-7, and d) B3PYMPM under different thicknesses in correspondence with Figure 2a–d. e) Relationship between the exciton recombination efficiency and the thickness of HBL for devices with different HBLs.

**ADVANCED
SCIENCE NEWS**

www.advancedsciencenews.com

**ADVANCED
MATERIALS
INTERFACES**

www.advmatinterfaces.de

the emitter, and the outcoupling efficiency, respectively. Φ_{out} is assumed to be 20% for devices on glass substrate without any light outcoupling enhancement, and Φ_{spin} and Φ_{PL} are 97% and 40%, respectively, according to the literature.[24] Figure 3e and Table 2 present the exciton recombination efficiency for different devices. The exciton recombination efficiency as the thickness of Bphen increases from 10 to 40 nm. TPBi based devices exhibit similar phenomena where the EQE and the exciton recombination efficiency increase gradually from 0.11% to 0.56% and from 1.3% to 6.3%, respectively. However, as for OXD-7 based devices, the brightness reaches a maximum of ≈850 cd m^{-2} and the EQE becomes saturated around 1.2% as the thickness increases to 30 nm. Further increasing the thickness to 40 nm leads to an abrupt drop of the brightness to ≈500 cd m^{-2} due to the apparent decreased drain current (Figure 2c). The saturation of EQE indicates that the hole blocking effect is not the sole factor contributing to a high EQE. We speculate that the inefficient electron transport in thick OXD-7 due to its low electron mobility (Table 1) is responsible for the saturation of EQE. This can be further verified by the fact that the EQE for B3PYMPM based devices show an obvious decrease from ≈1.2% to ≈1.0% as the thickness of B3PYMPM increases from 30 to 40 nm. B3PYMPM has a low electron mobility similar to that of OXD-7; meanwhile, it has much larger LUMO level gap (0.75 eV) between TBPMCN than that of OXD-7 (0.4 eV), which results in an inferior electron injection to TBPMCN, leading to the decrease of EQE at large thickness.

It is worth noting that the EQE for OXD-7 and B3PYMPM based devices are more than two times higher than that for Bphen and TPBi based devices. The much-improved maximum exciton recombination efficiency from ≈6.5% for Bphen and TPBi based devices to ≈16% for OXD-7 and B3PYMPM based

devices suggests that the balance between holes and electrons has been greatly improved. The above results also indicate that both the hole blocking and the electron transport process could make a significant influence on the balance of the carriers. This is quite different from the case in the OLEDs, where the carriers are more balanced and the exciton recombination efficiency can be assumed to be 100% for most cases.[24,33,34] Due to the well maintained balance of the carriers, the influence of HBL thickness is also less conspicuous in the OLEDs. Additionally, hole blocking in the OLEDs happens only in one direction which could be assumed as what happens beneath the drain electrode in the OLETs, whereas as shown in Figure 1b, two opposite directions of hole blocking have to be considered simultaneously in the OLETs. Thus, more comprehensive considerations of the HBL properties are required for building efficient multilayer OLETs.

Encouraged by the superior performance achieved by the HBL of OXD-7, we further fabricated multilayer OLETs with an efficient phosphorescent emitter of Fac-tris(2-phenylpyridinato) iridium(III) (Ir(ppy)$_3$) doped (6 wt%) CBP: ITO/PVP/PS/pentacene/NPB/HAT-CN/CBP:Ir(ppy)$_3$/OXD-7 (20 nm)/Cs$_2$CO$_3$/Al/Ag. For comparison, devices with the HBL of Bphen (20 nm) were also fabricated. **Figure 4** presents the electrical and optical characteristics for both devices. Both the transfer curves (Figure 4a) and output curves (Figure 4c,d) show similar p-type characteristics with a hole mobility of 0.14 and 0.12 cm^2 V^{-1} s^{-1} and a threshold voltage of −27.9 and −39.3 V for Bphen and OXD-7 based devices, respectively. The lower hole mobility and higher threshold voltage for OXD-7 based devices are anticipated due to the existence of a greater hole blocking effect beneath both the source and the drain electrodes. Nevertheless, they exhibit a maximum brightness of ≈8000 cd m^{-2} which
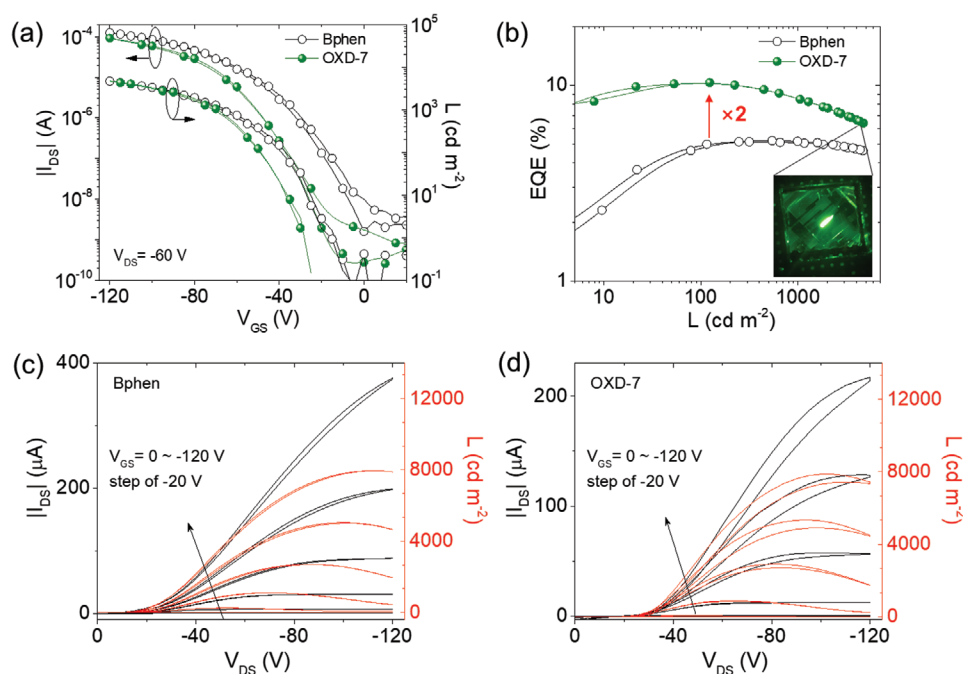

Figure 4. Electrical and optical characteristics for CBP:Ir(ppy)$_3$ based devices with the HBL of Bphen and OXD-7: a) transfer curves at $V_{DS} = -60$ V for both devices. b) EQE and brightness in correspondence with (a), inset is the image of an operating device with the HBL of OXD-7. Output curves for c) Bphen and d) OXD-7 based devices.

Table 3. Summary of device performance in literatures for multilayer OLETs with EQE greater than 1%.

Ref.	Typical voltage [V]	Mobility [cm^{-2} V^{-1} s^{-1}]		On/off ratio	Wavelength		L_{max} [cd m^{-2}]	EQE$_{max}$ [%]
		μ_h	μ_e		Color	Peak [nm]		
[41]	10	2	–	10^4	Blue	440	675	1.1
[15]	100	0.12	0.003	10^5	Yellow	–	2100	1.9
[7]	100	0.014	–	10^4	Blue	440	650	2.1
[19]	100	0.1	0.08	10^2	Yellow	–	1000	2.1
[11]	100	0.11	–	10^4	Yellow	555	1890	3.76
[16]	100	1.28	–	10^5	Green	514	8350	4.7
[18]	100	0.08	0.5	10^3	Red	600	–	5
[45]	30	1	0.1	10^5	Red	628	2190	5.7
[46]	24	1.45	–	10^5	Green	525	14 500	9
This work	100	0.12	–	10^5	Green	514	8000	10.3
	100	0.29	–	10^5	Blue	442	855	1.39

is comparable to that of Bphen based devices. This leads to approximately two times enhancement of the maximum EQE from 5.1% to 10.3% for OXD-7 based devices compared to that of Bphen based devices (Figure 4b). The EQE can well maintain above 8% at a brightness of 1000 cd m^{-2}, representing a relatively low efficiency roll-off.

In addition to the balance of the carriers, it should be noted that an HBL with high triplet energy (T1) is also critical for phosphorescent EL devices as the energy of triplet excitons may transfer from the emitter to the HBL through the Dexter process.[35,36] The T1 of OXD-7 is 2.70 eV,[37] which is much higher than that of CBP (2.56 eV)[38] and Ir(ppy)$_3$ (2.42–2.46 eV),[38,39] while Bphen has a relatively lower T1 of 2.50 eV.[40] Therefore, the higher-lying of T1 for OXD-7 may also contribute to the better EQE than that of Bphen for the phosphorescent OLETs, which is worth further study in the future. As summarized in **Table 3**, the performance of our devices, especially the EQE which exceeds 10% for the first time, is among the best results reported for multilayer OLETs, highlighting the merits of the strategy of exploring the hole blocking effect. Though the operation voltages are high for current devices, they could be reduced by adopting insulating materials with high dielectric constant.[41,42] Besides, strategies such as shortening the channel length[43] and modifying the charge transport layer with low defects[44] would also be beneficial in reducing the operation voltages.

3. Conclusion

In summary, we have demonstrated that the HBL plays a crucial role in the performance of multilayer OLETs. It has been found that the HBL with a deeper HOMO level can better facilitate the hole blocking effect to promote the exciton recombination efficiency and EQE. The HBL not only blocks the holes but also affects the transport of electrons, leading to the dependence on the thickness and the LUMO level of the HBL, especially for HBL materials with low electron mobilities. By using OXD-7 as the HBL, a high EQE of 1.39% has been achieved in a blue fluorescent OLET, and an EQE exceeding 10% has been achieved

for the first time in a green phosphorescent OLET. Our results may provide a new sight for the structure design and material choice for future efficient OLETs.

4. Experimental Section

Materials: PVP, PS, and Cs$_2$CO$_3$ (99.99%) were purchased from Sigma-Aldrich. Pentacene was purchased from Banhe Tec. HAT-CN was purchased from Shanghai Han Feng Chemical Co., Ltd. CBP, Ir(ppy)$_3$, NPB, OXD-7, TPBi, Bphen, and B3PYMPM were purchased from Xi'an Polymer Light Technology Corp. All materials were used as received without further purification. TBPMCN was synthesized as previously reported.[24]

Device Fabrication: ITO glass substrates were ultrasonically cleaned with acetone, alcohol, and deionized water in sequence. The PVP (500 nm) was spun coated onto ITO glass substrates using solution prepared with PVP and poly(melamine-*co*-formaldehyde) (2:1 wt%) in propylene glycol monomethyl ether acetate (90 mg mL^{-1}) and then annealed at 200 °C for 1 h. The PS (30 nm) dissolved in toluene (6 mg mL^{-1}) was successively spun coated (30 s at 3000 rpm) on PVP and annealed at 85 °C for 1 h. Pentacene (14 nm), NPB (10 nm), HAT-CN (1 nm), emission layer (TBPMCN or CBP:Ir(ppy)$_3$, 30 nm), HBL (Bphen or TPBi or OXD-7 or B3PYMPM), Cs$_2$CO$_3$ (1 nm), and Al (1 nm) were successively thermal evaporated with the rate of 0.2, 0.3, 0.1, 2, 0.3, 0.2, and 0.2 Å s^{-1}, respectively. Ag (50 nm) was thermally deposited through a shadow mask with channel length and width of 60 and 3000 μm, respectively. All the devices were encapsulated with UV glue in the glovebox (H$_2$O, O$_2$ < 0.1 ppm) before testing. The light emission was detected from the ITO side.

Film and Device Characterizations: The thickness of the films was calibrated using a surface profiler (XP-1, Ambios). The UV–vis–NIR absorption spectra were performed with a Shimadzu UV-3101 PC spectrophotometer. PL spectra were measured using Hitachi florescence spectrometer F-7000. The atomic force microscopy measurement was performed on a Shimadzu SPM-9700 under the phase mode.

The electrical characteristics of OLETs were performed by Keithley 4200 SCS at room temperature under air ambient. The photocurrent was recorded by HAMAMATSU S1336 photodiode. The optical images were captured by Olympus BX51TRF charge-couple device microscope. The electroluminescence spectra were measured by AvaSpec-ULS2048L fiber spectrometer. The luminance for OLETs was calculated by comparing the photocurrent with the fabricated OLEDs at fixed luminance (500 cd m^{-2}) and emission area (1 mm × 1.5 mm). The EQE for OLETs was calculated from the luminance, the drain current, and the EL emission spectrum assuming Lambertian emission.

Supporting Information

Acknowledgements

Conflict of Interest

The authors declare no conflict of interest.

Keywords

[1] J. Zaumseil, *Adv. Funct. Mater.* **2019**, *30*, 1905269.
[2] C. C. Zhang, P. L. Chen, W. P. Hu, *Small* **2016**, *12*, 1252.
[3] M. Schidleja, C. Melzer, H. von Seggern, *Adv. Mater.* **2009**, *21*, 1172.
[4] M. U. Chaudhry, K. Muhieddine, R. Wawrzinek, J. Li, S.-C. Lo, E. B. Namdas, *ACS Photonics* **2018**, *5*, 2137.
[5] B. Walker, M. Ullah, G. J. Chae, P. L. Burn, S. Cho, J. Y. Kim, E. B. Namdas, J. H. Seo, *Appl. Phys. Lett.* **2014**, *105*, 183302.
[6] M. Ullah, Y. H. Lin, K. Muhieddine, S. C. Lo, T. D. Anthopoulos, E. B. Namdas, *Adv. Opt. Mater.* **2016**, *4*, 231.
[7] M. Ullah, K. Tandy, A. J. Clulow, P. L. Burn, I. R. Gentle, P. Meredith, S. C. Lo, E. B. Namdas, *ACS Photonics* **2017**, *4*, 754.
[8] Z. S. Qin, H. K. Gao, J. Y. Liu, K. Zhou, J. Li, Y. Y. Dang, L. Huang, H. X. Deng, X. T. Zhang, H. L. Dong, W. P. Hu, *Adv. Mater.* **2019**, *31*, 1903175.
[9] T. Komori, H. Nakanotani, T. Yasuda, C. Adachi, *J. Mater. Chem. C* **2014**, *2*, 4918.
[10] E. B. Namdas, B. B. Hsu, Z. Liu, S. C. Lo, P. L. Burn, I. D. Samuel, *Adv. Mater.* **2009**, *21*, 4957.
[11] L. Song, Y. Hu, Z. Liu, Y. Lv, X. Guo, X. Liu, *ACS Appl. Mater. Interfaces* **2017**, *9*, 2711.
[12] J. Sobus, F. Bencheikh, M. Mamada, R. Wawrzinek, J. C. Ribierre, C. Adachi, S. C. Lo, E. B. Namdas, *Adv. Funct. Mater.* **2018**, *28*, 1800340.
[13] G. Q. Tang, B. J. Li, J. B. Lan, J. S. You, *Adv. Mater. Interfaces* **2017**, *4*, 1700453.
[14] K. Muhieddine, M. Ullah, F. Maasoumi, P. L. Burn, E. B. Namdas, *Adv. Mater.* **2015**, *27*, 6677.
[15] M. Ullah, K. Tandy, S. D. Yambem, M. Aljada, P. L. Burn, P. Meredith, E. B. Namdas, *Adv. Mater.* **2013**, *25*, 6213.
[16] L. Song, Y. Hu, N. Zhang, Y. Li, J. Lin, X. Liu, *ACS Appl. Mater. Interfaces* **2016**, *8*, 14063.
[17] J. H. Seo, E. B. Namdas, A. Gutacker, A. J. Heeger, G. C. Bazan, *Adv. Funct. Mater.* **2011**, *21*, 3667.
[18] R. Capelli, S. Toffanin, G. Generali, H. Usta, A. Facchetti, M. Muccini, *Nat. Mater.* **2010**, *9*, 496.
[19] M. Ullah, K. Tandy, S. D. Yambem, K. Muhieddine, W. J. Ong, Z. Shi, P. L. Burn, P. Meredith, J. Li, E. B. Namdas, *Org. Electron.* **2015**, *17*, 371.
[20] K. Tandy, M. Ullah, P. L. Burn, P. Meredith, E. B. Namdas, *Org. Electron.* **2013**, *14*, 2953.
[21] A. P. Kulkarni, C. J. Tonzola, A. Babel, S. A. Jenekhe, *Chem. Mater.* **2004**, *16*, 4556.
[22] Y. Shirota, H. Kageyama, *Chem. Rev.* **2007**, *107*, 953.
[23] B. B. Y. Hsu, J. Seifter, C. J. Takacs, C. M. Zhong, H. R. Tseng, I. D. W. Samuel, E. B. Namdas, G. C. Bazan, Y. Fei, Y. Cao, A. J. Heeger, *ACS Nano* **2013**, *7*, 2344.
[24] S. T. Zhang, L. Yao, Q. M. Peng, W. J. Li, Y. Y. Pan, R. Xiao, Y. Gao, C. Gu, Z. M. Wang, P. Lu, F. Li, S. J. Su, B. Yang, Y. G. Ma, *Adv. Funct. Mater.* **2015**, *25*, 1755.
[25] S. Lee, J. H. Lee, J. H. Lee, J. J. Kim, *Adv. Funct. Mater.* **2012**, *22*, 855.
[26] T. Yasuda, Y. Yamaguchi, D.-C. Zou, T. Tsutsui, *Jpn. J. Appl. Phys.* **2002**, *41*, 5626.
[27] S. Naka, H. Okada, H. Onnagawa, T. Tsutsui, *Appl. Phys. Lett.* **2000**, *76*, 197.
[28] W.-Y. Hung, T.-H. Ke, Y.-T. Lin, C.-C. Wu, T.-H. Hung, T.-C. Chao, K.-T. Wong, C.-I. Wu, *Appl. Phys. Lett.* **2006**, *88*, 064102.
[29] H. Sasabe, D. Tanaka, D. Yokoyama, T. Chiba, Y.-J. Pu, K.-I. Nakayama, M. Yokoyama, J. Kido, *Adv. Funct. Mater.* **2011**, *21*, 336.
[30] H.-S. Seo, D.-K. Kim, J.-D. Oh, E.-S. Shin, J.-H. Choi, *J. Phys. Chem. C* **2013**, *117*, 4764.
[31] S. Kahmann, A. Shulga, M. A. Loi, *Adv. Funct. Mater.* **2019**, *30*, 1904174.
[32] T. Earmme, S. A. Jenekhe, *J. Mater. Chem.* **2012**, *22*, 4660.
[33] Y.-H. Chen, D.-G. Ma, H.-D. Sun, J.-S. Chen, Q.-X. Guo, Q. Wang, Y.-B. Zhao, *Light: Sci. Appl.* **2016**, *5*, e16042.
[34] X. Ai, E. W. Evans, S. Dong, A. J. Gillett, H. Guo, Y. Chen, T. J. H. Hele, R. H. Friend, F. Li, *Nature* **2018**, *563*, 536.
[35] C. Y. Xiang, W. Koo, F. So, H. Sasabe, J. Kido, *Light: Sci. Appl.* **2013**, *2*, e74.
[36] Y. J. Kang, J. Y. Lee, *Org. Electron.* **2016**, *32*, 109.
[37] S. Tokito, M. Suzuki, F. Sato, M. Kamachi, K. Shirane, *Org. Electron.* **2003**, *4*, 105.
[38] H. Inomata, K. Goushi, T. Masuko, T. Konno, T. Imai, H. Sasabe, J. J. Brown, C. Adachi, *Chem. Mater.* **2004**, *16*, 1285.
[39] X. F. Ren, J. Li, R. J. Holmes, P. I. Djurovich, S. R. Forrest, M. E. Thompson, *Chem. Mater.* **2004**, *16*, 4743.
[40] N. Chopra, J. Lee, Y. Zheng, S.-H. Eom, J. Xue, F. So, *ACS Appl. Mater. Interfaces* **2009**, *1*, 1169.
[41] M. Ullah, R. Wawrzinek, F. Maasoumi, S.-C. Lo, E. B. Namdas, *Adv. Opt. Mater.* **2016**, *4*, 1022.
[42] Y. J. Park, A. Song, B. Walker, J. H. Seo, K. B. Chung, *Adv. Opt. Mater.* **2019**, *7*, 1801290.
[43] B. Kumar, B. K. Kaushik, Y. S. Negi, *Polym. Rev.* **2014**, *54*, 33.
[44] K. P. Pernstich, S. Haas, D. Oberhoff, C. Goldmann, D. J. Gundlach, B. Batlogg, A. N. Rashid, G. Schitter, *J. Appl. Phys.* **2004**, *96*, 6431.
[45] J.-H. Lee, T.-H. Ke, J. Genoe, P. Heremans, C. Rolin, *Adv. Electron. Mater.* **2019**, *5*, 1800437.
[46] H. Chen, X. Xing, J. Miao, C. Zhao, M. Zhu, J. Bai, Y. He, H. Meng, *Adv. Opt. Mater.* **2020**, *8*, 1901651.